Small-Scale Wind Disturbances Observed by the MU Radar during the Passage of Typhoon Kelly

KAORU SATO

Department of Geophysics, Faculty of Science, Kyoto University, Kyoto, Japan

(Manuscript received 14 December 1990, in final form 10 February 1992)

ABSTRACT

This paper describes small-scale wind disturbances associated with Typhoon Kelly (October 1987) that were observed by the MU radar, one of the MST (mesosphere, stratosphere, and troposphere) radars, continuously for about 60 hours with fine time and height resolution. First, in order to elucidate the background of small-scale disturbances, synoptic-scale variation in atmospheric stability related to the typhoon structure during the observation is examined. When the typhoon passed near the MU radar site, the structure was no longer axisymmetric. There is deep convection only in the front (north-northeast) side of the typhoon while convection behind it is suppressed by a synoptic-scale cold air mass moving eastward to the west of the typhoon. A drastic change in atmospheric stability over the radar site as indicated by echo power profiles is likely due to the passage of the sharp transition zone of convection.

Strong small-scale wind disturbances were observed around the typhoon passage. It is shown that the statistical characteristics are significantly different before (BT) and after (AT) the typhoon passage, especially in frequency spectra of vertical wind fluctuations. The spectra for BT are unique compared with earlier studies of vertical winds observed by VHF radars. Another difference is dominance of a horizontal wind component with a vertical wavelength of about 3 km, which is observed only in AT.

Further analyses are made of detailed characteristics and vertical momentum fluxes for dominant disturbances. It is found that some of the disturbances are generated so as to remove the momentum of cyclonic wind rotation of the typhoon. Deep convection, topographic effects in strong winds, and strong vertical shear of horizontal winds around an inversion layer are possible sources of the dominant disturbances. Moreover, two monochromatic disturbances lasting for more than 10 h in the lower stratosphere observed in BT and AT, respectively, are identified as inertio–gravity waves, by obtaining wave parameters consistent with all observed quantities. Both of the inertio–gravity waves propagate energy away from the typhoon.

1. Introduction

One of the most important issues on gravity waves is the energy sources and generation mechanisms. Observational studies of gravity waves have been performed widely since the 1950s. Uccellini and Koch (1987) reviewed the earlier studies using conventional tools and suggested that shearing instability and geostrophic adjustment in synoptic-scale wind systems are possible source mechanisms. Due to limitations on resolution of the observational tools, however, the analyses have been restricted to gravity waves with comparatively large scales (horizontal wavelengths of tens to hundreds of kilometers). Recently advanced MST radars (VHF/UHF clear-air Doppler radars) provide wind velocities with fine time and height resolution, which enable us to investigate detailed structures of small-scale gravity waves in a wide range of frequency and vertical wavenumber spectra. With the aid of the MST radars, several kinds of gravity waves were detected and the relation to synoptic-scale atmospheric phenomena was discussed in some studies. Hirota and Niki (1986) found inertio–gravity waves propagating upward and downward from the subtropical westerly jet in winter. Fukao et al. (1989) showed strong wind fluctuations like gravity waves associated with a cold vortex (a cutoff cyclone). Sato (1989) detected an inertio–gravity wave generated near the tropopause due to shearing instability when a synoptic-scale pressure trough passed over the radar site. Another important generation mechanism of gravity waves is a topographic effect in strong surface wind. Although the topographically forced waves are quasi-stationary, MST radars can observe the phase fluctuations caused by changes of the background wind as temporal fluctuations, especially in vertical winds (Ecklund et al. 1981, 1982, 1985, 1986; Sato 1990). According to these studies and others using aircraft (e.g., Lilly and Kennedy 1973; Lilly et al. 1982; Brown 1983; Hoinka 1984, 1985), the topographically forced waves are accompanied by large vertical momentum flux.

Tropical cyclones are also fascinating mesoscale energy sources of gravity waves. They have been examined in relation to gravity waves especially for the for-

Corresponding author address: Dr. Kaoru Sato, Kyoto University, Department of Geophysics, Kyoto, 60601, Japan.

mation of spiral rainbands, which are conventionally explained to be a manifestation of internal gravity waves (e.g., Yamamoto 1963; Abdullah 1966; Kurihara 1976; Xu 1983). Recent studies with aircraft observations (Willoughby et al. 1984) and a three-dimensional numerical model (Yamasaki 1986) show that not all features of the spiral bands are consistent with gravity waves, while some propagating bands are considered to be due to inertio-gravity waves. Gravity waves have various horizontal and vertical scales in a wide range. Generation of small-scale intense gravity waves related to the typhoon that are forced topographically in strong wind near the ground and are associated with strong convection can be expected as well as those with larger scales of spiral rainbands. There have been only a few observational studies on such small-scale gravity waves, however. Black (1977, 1983) analyzed stereoscopic photographs from Skylab of a hurricane and detected small-scale structures like gravity waves with wavelength of 1.5–13 km on the periphery of a deep convective cloud around the tropopause. He attributed the generation mechanism of gravity waves to deep penetration of convection striking a stable layer aloft. Matsumoto and Okamura (1985) detected a sharp pressure dip accompanied with a typhoon using data from a dense network of surface meteorological observations and a Doppler radar around the Kanto District in Japan, and showed that the structure of the pressure dip is consistent with an internal gravity wave. Hung et al. (1988) made a wind observation by an MST radar located at Chung Li, Taiwan, for about one hour and detected some gravity waves. Statistical characteristics of small-scale wind disturbances could not be shown because of insufficient observation time.

A 60-hour continuous wind observation of Typhoon Kelly was successfully performed in October 1987 with the MU radar at Shigaraki, Shiga, Japan (35°N, 136°E). Quality of the data is sufficiently high for examinations of small-scale disturbances in terms of the observational period and resolution. Some results obtained by a preliminary analysis of the data have already been reported by Sato et al. (1991, hereafter referred to as S91). Strong vertical wind fluctuations with short periods of several tens of minutes, and dominant gravity waves with a short vertical wavelength of about 3 km and periods longer than 10 h, were also reported.

There are several remaining but important issues on small-scale disturbances associated with a typhoon, however, that can be first investigated with the aid of such data of high quality. These include elucidating spectral structures of the disturbances in comparison with those in other synoptic situations, describing detailed characteristics of several dominant disturbances, and examining interactions between the disturbances and typhoon quantitatively through the analysis of vertical momentum flux, which can be calculated directly from the MU radar wind data.

Description of the data appears in section 2. In section 3, the structure of the typhoon as the "background" of small-scale disturbances is examined. Statistical characteristics of the disturbances are shown in section 4. An analysis of vertical momentum flux is introduced in section 5, which is a key in the following investigations in sections 6–9 for several dominant disturbances in terms of characteristics, possible sources, and effects on the typhoon. Summary and concluding remarks are made in section 10.

2. Data description

Wind observations were made every 2.5 min during about 60 hours from 2206 LST (Local Standard Time) 15 to 0916 LST 18 October 1987 (all date-times are in October) with the MU radar operating at 46.5 MHz. Line-of-sight wind velocities were measured by five beams directed vertically and tilted to the north, east, south, and west with the same zenith angle of 10°. The resolution of the line-of-sight velocity is less than 0.1 m s^{-1} when signal-to-noise ratio of the echo is sufficiently high. The observed height range is about 2–25 km with a spatial resolution of 150 m along the respective beam directions. Details of the system of the MU radar have been given by Fukao et al. (1985a,b).

3. Typhoon structure as the background of small-scale disturbances

Figure 1 shows the track of Typhoon Kelly. The typhoon with the minimum surface center pressure of 955 hPa recurved and began to weaken about 24–30

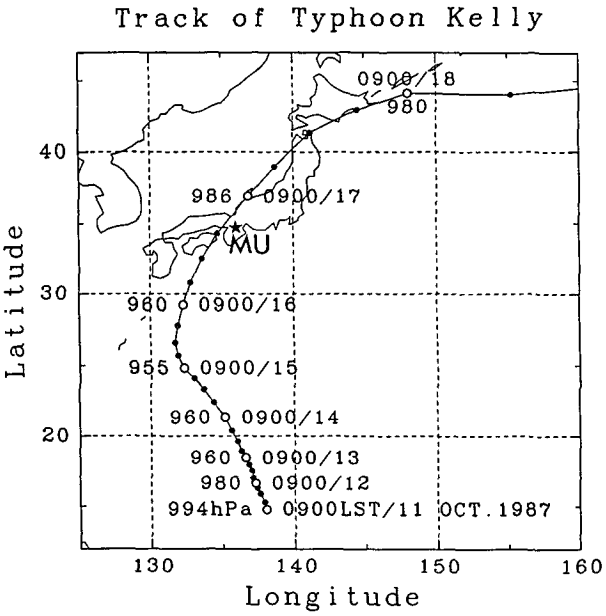

FIG. 1. The track of Typhoon Kelly. Note that Local Standard Time (UTC − 9 h) is used.

h before the center reached the coast of Japan and west of the MU radar site. The closest distance between the typhoon center and the radar site was about 100 km around 0500 LST 17 when the surface center pressure was about 980 hPa. Transformation into an extratropical cyclone was completed at 2100 LST 17. Thus, roughly speaking, the MU radar scanned from the northeast to the southwest of the typhoon over a distance of around 2000 km while the typhoon was gradually weakened and transformed into an extratropical cyclone.

Series of surface weather maps, satellite IR pictures, and precipitation maps at an interval of 12 h around the time that the typhoon passed near the radar site are presented in Fig. 2. Here the precipitation maps were made by the Japan Meteorological Agency (JMA) using raingage data obtained by a surface meteorological network, Automated Meteorological Data Acquisition System (AMeDAS), and echo data of meteorological radars. At 0900 LST 16, clouds in spiral shapes are associated with the typhoon and a stationary front is formed between warm air of the typhoon and cold midlatitude air to the south of Japan corresponding to a rainband. The spiral-shaped clouds disappeared by 2100 LST 16 and bright, that is, high clouds are observed only to the north-northeast area of the typhoon. The cloud patterns are consistent with the rainfall map, which shows that convective rain more than 16 mm h^{-1} was observed only in the front side of the typhoon and little precipitation was observed behind it except for very weak rain in the southwest region. This indicates that the convective activity over the MU radar site was much more intense in the period before the typhoon passage (BT) than after (AT) on the whole. It should be noted that the boundary seen in the cloud and precipitation distributions is sharp. The boundary was also observed at 0900 and 2100 LST 17 from northwest to southeast of the typhoon, and became an occluded front at 0900 LST 18 (not shown).

Horizontal wind vectors observed by the MU radar are shown in Fig. 3. In order to see the outline of wind variation associated with the typhoon, the data were smoothed by low-pass filters with cutoff lengths of 3 km in vertical and 3 h in time. Strong northward winds were observed at lower levels around the time of typhoon passage (indicated by a thick arrow) and 6 h later the wind shifted to southeastward. The wind pattern is consistent with the northward motion of the center of the typhoon to the west of the MU radar site. It is noted that winds above about 8 km are affected by the subtropical westerly jet.

Figure 4 is a time–height section of the echo power of the beam tilted toward the north. Echo power received by the VHF radars shows the turbulence intensity weighted by the potential refractive index gradient (e.g., Hocking 1985). Roughly speaking, the variation in echo power is indicative of change in atmospheric stability. The tropopause is seen at a height of 16.5 km as a vertical discontinuity of the echo power. A temporal discontinuity is observed in the whole troposphere at the passage of the typhoon center (0500 LST 17). This corresponds to the sharp transition zone between a region with deep convection to the north-northeast of the typhoon and a relatively cloud-free region to the south-southwest, as observed in Fig. 2.

Figure 5 shows time series of rainfall rate made from the Radar–AMeDAS composite data at two locations about 2.5 km north-northeast and west-southwest of the radar site, respectively. During the observation period, there was no intense rainfall around the MU radar site except for two peaks. The first peak observed around 1900 LST 16 in BT is probably due to deep convection in the north-northeast side of the typhoon, although the amount of rainfall is not large. The second peak around 0700 LST 17 in early AT, which lasted longer than the first one, is likely due to local orographic rainfall, because the peak is related to a topographically fixed rainfall system having a diameter of about 100 km that gradually weakened while typhoon passed away (not shown in detail).

It is worth noting about Fig. 4 that a conspicuous layer with strong echo power is rising up gradually from a height of 5 km to 9.5 km in AT. This layer corresponds to an inversion layer and a sharp gradient of humidity (S91). Figure 6 shows vertical profiles of temperature anomaly from an vertically smoothed profile of the average for the nine as a reference (shown on the right), obtained using data with radiosondes launched at the radar site. It is found that the lower-tropospheric region below the inversion layer was colder by several degrees. This is probably due to the surge of cold air mass from higher latitudes that suppressed deep convection behind the typhoon. Since the inversion layer lasted over one day at the radar site, the layer must have a synoptic-scale horizontal structure. In fact, similar inversion layers were observed at Shionomisaki (33°N, 135°E), Yonago (35°N, 133°E), Fukuoka (33°N, 130°E), and Hamamatsu (34°N, 137°E), located around the same latitude of the MU radar site where routine balloon observations are made every 0900 and 2100 LST (not shown). The inversion layer got thicker and rose up later, and the lowest height of 11–12 km was recognized as the tropopause at 0900 LST 20 at Yonago, Fukuoka, and Hamamatsu. Thus, it can be said that the inversion layer observed at the radar site corresponds to the extratropical tropopause and the tropopause at a height of 16.5 km is the tropical tropopause.

4. Difference in statistical characteristics of wind disturbances between BT and AT

In the previous section it was shown that the atmospheric stability (convective activity) over the radar site is considerably different between BT and AT. The

FIG. 2. (a) Synoptic charts of sea-level pressure in hectopascal, (b) IR pictures of GMS, and (c) the Radar–AMeDAS composite charts presenting precipitation per hour. Numerals in the top left of each figure in (a) denote local time and date. The typhoon center is indicated by "T" in (a) and (c), and by thick arrows in (b). Circles show the location of the MU radar. Dash-dotted lines in (c) show the boundaries in which the precipitation data exist.

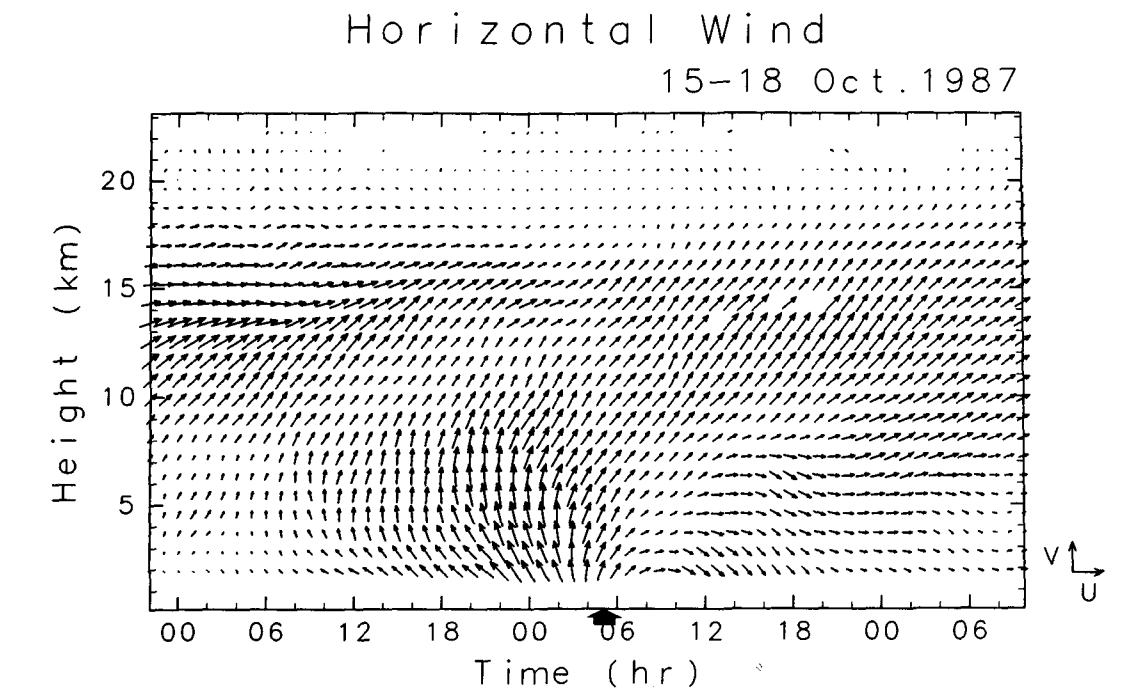

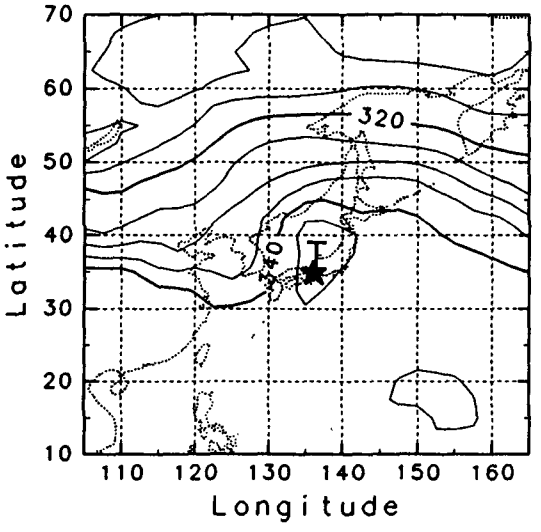

FIG. 3. A time–height section of horizontal wind vectors observed by the MU radar. Rightward and upward unit vectors show zonal (U) and meridional (V) winds of 50 m s^{-1}, respectively. A thick arrow on the horizontal axis denotes the time when the typhoon passed near the MU radar site.

characteristics of small-scale wind disturbances are possibly influenced by the difference.

Figure 7 presents a time–height section of vertical winds (w) observed using the vertical beam. The estimated vertical winds in the lower height region may be in error when there is heavy rainfall because of contamination of echoes from falling raindrops. See Fukao et al. (1985c) and Wakasugi et al. (1986, 1987) for examples. As found from Fig. 5, there were two peaks of rainfall at around 1900 LST 16 and 0700 LST 17. During the periods the vertical winds below the melting level may be biased toward negative values. It can be shown as follows, however, that the contamination by rain echoes is not severe for the present data.

Intensity of the echo from raindrops is proportional to the sixth power of the drop diameter (Battan 1973). Thus, the 46.5-MHz MU radar observes strong rain echo, which is comparable to or slightly stronger than the atmospheric turbulence echo at the most, only when the rain contains large drops with large fall speeds of about 5 m s^{-1}. This shows that vertical profiles and/or time series of vertical winds degraded severely by the rain echo must have gaps larger than about 5 m s^{-1} between adjacent erroneous and correct estimates. The gaps are sufficiently large for detection. In the present data none of the wind profiles has such large gaps, indicating little contamination. On the other hand, echoes from snowflakes or ice crystals are much weaker

FIG. 4. A time–height section of echo power observed by a beam tilted to the north with a zenith angle of 10°. Contour interval is 5 dB. A thick arrow on the horizontal axis denotes the time when the typhoon passed near the MU radar site.

than rain echoes, because refractive index of ice is small, and thus hardly affects velocity estimation. This is the case for the present data, which are not degraded severely even by rain echoes.

Vertical wind disturbances with amplitudes of more than 1 m s^{-1} are seen for about 40 h around the typhoon passage. As expected, a temporal discontinuity in characteristics of the disturbances is found at the typhoon passage: dominant periods of the disturbances in BT are much shorter than in AT. The disturbances are seen in the whole observed height region in BT, while large vertical wind fluctuations are confined below the tropopause in AT. It should be noted that the characteristics of vertical wind disturbances do not depend strongly on the existence of local heavy rainfall (see Fig. 5).

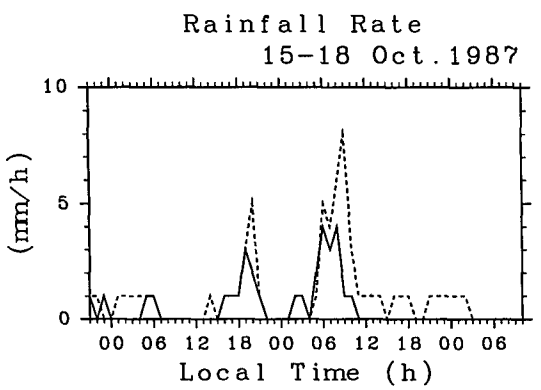

FIG. 5. Time series of rainfall rate at two locations about 2.5 km north-northeast (a solid curve) and about 2.5 km west-southwest (a dashed curve) to the MU radar site, respectively. Time resolution is one hour.

In order to examine the difference in time scales of disturbances between BT and AT in detail, frequency power spectra of w are calculated for the two periods from 1400 LST 16 to 0200 LST 17 for BT and from 0800 to 2000 LST 17 for AT. Figure 8 shows the spectra in the energy content form for different height ranges. Solid and dotted lines present the spectra of w in BT and AT, respectively. Power spectra are averaged in three height regions, namely, 5.5–9, 9–16, and 16–20 km, which are discriminated by difference in thickness of the lines. The boundaries of 9 and 16 km correspond to the heights of the inversion layer observed in AT and the tropopause, respectively. The data below 5.5 km are not used in order to avoid the contamination of rainfall. Smoothing is made for the spectral densities in the frequency domain. An error bar in Fig. 8 shows a 95% confidence interval of the spectra. For estimation

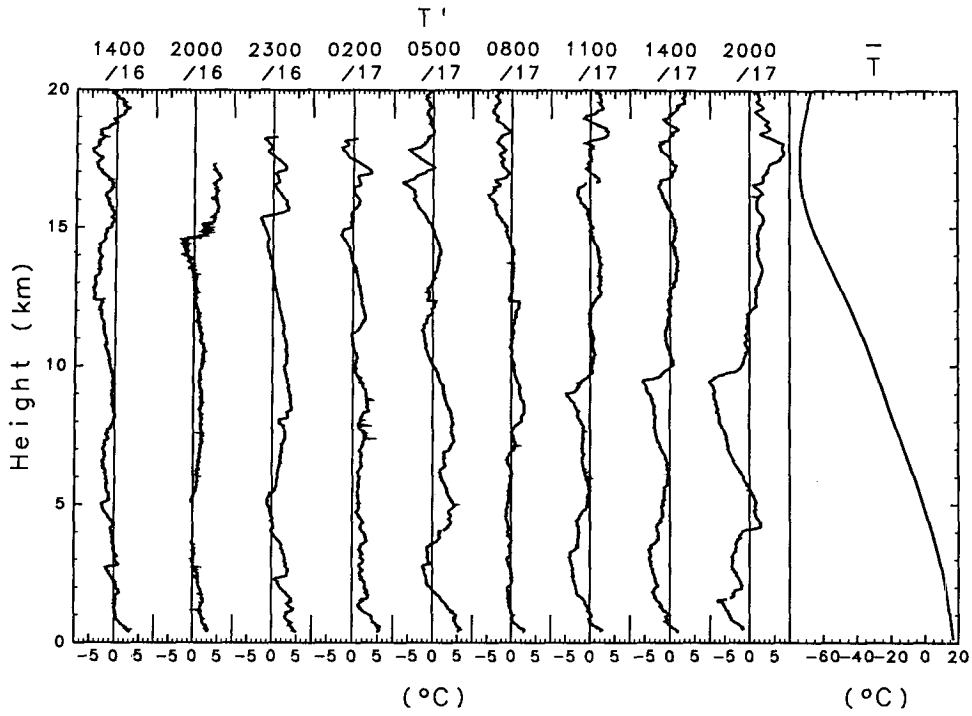

FIG. 6. A time series of temperature anomaly (T') and the reference profile ($\bar{T}$). Numerals on the top denote local time and date.

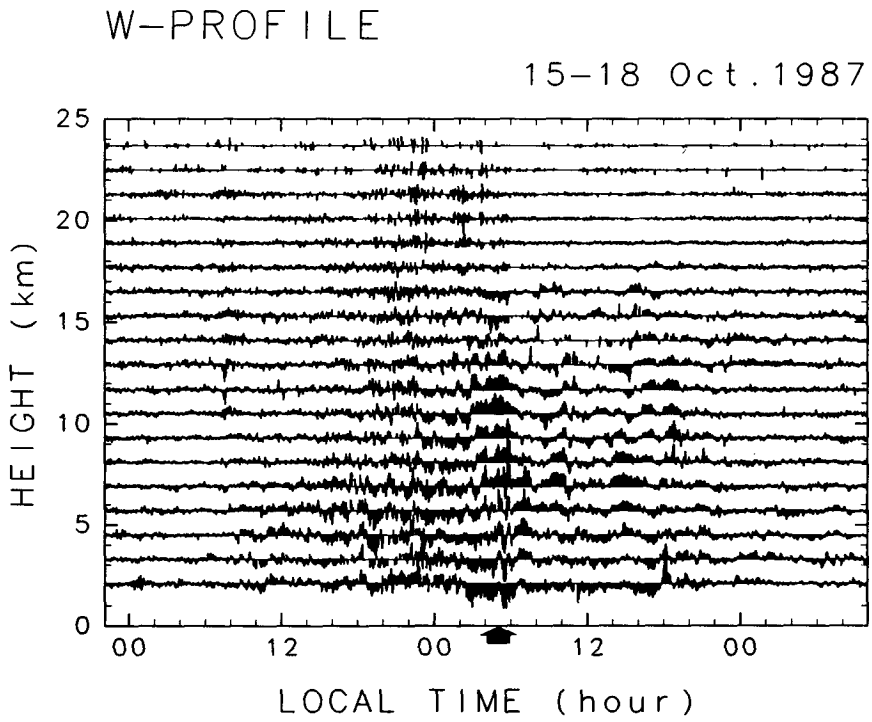

FIG. 7. The vertical wind profile as a function of height measured with a vertical beam during 15–18 Oct 1987. The spacing of horizontal lines shows velocity of 3 m s^{-1}. A thick arrow on the horizontal axis shows the time when a center of the typhoon passed near the MU radar site.

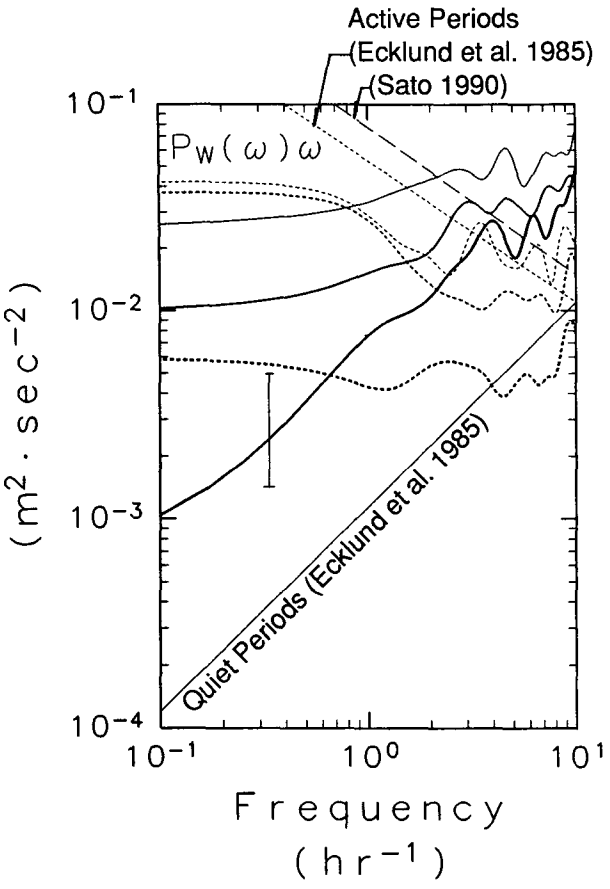

FIG. 8. Power spectra of vertical wind fluctuations observed in BT (solid lines) and AT (dotted lines) in the energy content form. Thin, thick, and very thick lines show the spectra for height regions of 5.5–9, 9–16, and 16–20 km, respectively. Straight lines are spectra obtained by the other studies using VHF radars.

of the confidence interval, reduction of statistical noise by the vertical averaging was ignored. It is not easy to evaluate the effectiveness of the vertical averaging because the vertical wind fluctuations may have correlation in height to some extent. Thus, the spectra may be more accurate than shown by the error bar.

No distinct peaks are found in the spectra in both BT and AT. Inclination of power spectra in BT is larger than that in AT. The spectra of AT and BT cross around a frequency of 1 h^{-1} for all the height regions. Let us compare these spectra with those obtained using the VHF radars in earlier studies. Strong vertical wind fluctuations are observed in the troposphere and lower stratosphere recurring at several-day periods at various locations: Poker Flat, Alaska; the lee of the Colorado Rockies; and the Rhone delta, southern France (Ecklund et al. 1981, 1982, 1985, 1986). Ecklund et al. (1985, 1986) showed that frequency power spectra of w in periods when strong vertical wind fluctuations are observed (active periods) are in a shape of $\omega^{-5/3}$, whereas the spectra in periods when there are little vertical wind fluctuations (quiet periods) have a shape of ω^0. Sato (1990) made an analysis of vertical wind disturbances observed by the MU radar in late autumn and winter, and found that the power spectra are not necessarily in a shape of $\omega^{-5/3}$ but resemble the spectra analyzed for active periods by Ecklund et al. in a sense that the power is distributed largely to lower frequencies. From the correlation between vertical wind activity and horizontal wind near the surface, it was shown that the large vertical wind fluctuations are due to topographically forced gravity waves (Ecklund et al. 1982; Sato 1990). Dashed and solid thin straight lines in Fig. 8 are the spectra obtained by Ecklund et al. (1985) in a height range of 4–6 km for active and quiet periods, respectively. A dotted thin straight line is the spectrum in a height region of 15–20 km for active periods obtained by Sato (1990).

The spectra for AT in the troposphere resemble those for the active periods in both slope and magnitude of spectral densities. On the other hand, the spectra for BT are similar in slope to but significantly larger in magnitude than that in the quiet periods. Total power of vertical wind fluctuations in BT is rather similar to that in the active periods. Therefore, the spectral structure of vertical wind disturbances observed in BT is unique.

Vertical wavenumber spectra for horizontal wind components have been examined observationally and theoretically by several previous studies. Dewan and Good (1986) and Smith et al. (1987) suggested theoretically that the spectra for saturated gravity waves are proportional to N^2m^{-3}, where N is the Brunt–Väisälä frequency and m is vertical wavenumber. Tsuda et al. (1989) showed that the spectra obtained by the MU radar observations are in accord well with the spectral theory, although the theory contains unconfirmed assumption (Hines 1991).

Despite the dependence on the Brunt–Väisälä frequency, the vertical wavenumber spectra are examined for the whole observed height range in the present study because of insufficient length of data in the stratosphere for the calculation. Since the spectra are expected to be steep theoretically, the original series of wind data are prewhitened following Tsuda et al. (1989). Spectra of horizontal wind components are obtained ignoring the contribution of w to the line-of-sight wind velocities measured by the four tilted beams.

The results for AT and BT are shown in Fig. 9. Thick solid and dotted lines show the vertical wavenumber spectra of zonal (u) and meridional wind components (v), respectively. Thin solid and dashed straight lines show the spectra for saturated gravity waves expected by the spectral theory (Smith et al. 1987) for troposphere and stratosphere, respectively. Both spectra of horizontal wind components obtained for BT and AT are almost in accord with the theory except for ends of the spectra. It is noteworthy that there is a peak around a wavelength of 3 km in AT that is not observed

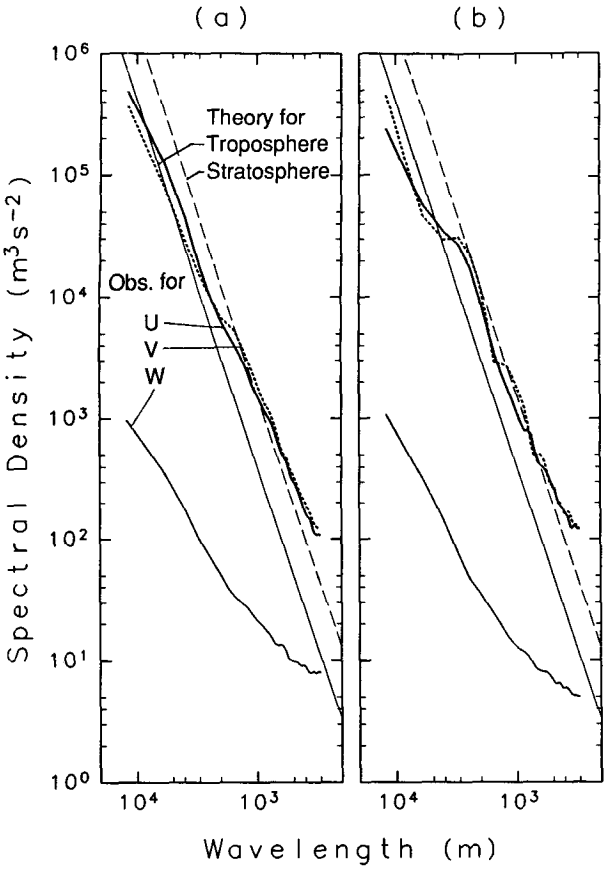

FIG. 9. Vertical wavenumber power spectra for (a) BT and (b) AT. Thick solid, thick dotted, and thin solid lines show the spectra of zonal, meridional, and vertical wind components, respectively. Dashed and solid straight lines are the spectra in the stratosphere and troposphere expected by a theory for saturated gravity waves, respectively.

in BT. Since a 95% confidence interval for the spectra is estimated at less than 5% assuming absence of coherent phenomena, the peak cannot be explained by statistical noise of the spectra. Thus, the peak indicates existence of monochromatic disturbances with the short wavelength only in AT that are probably identical to the gravity waves detected by S91. A thin solid line represents the vertical wavenumber spectra of w measured by a vertical beam. There is no large difference between BT and AT such as that observed in the frequency power spectra of w.

From the spectral analysis, it was found that there were three dominant disturbances during the observation: vertical wind disturbances with short periods in BT, vertical wind disturbances with long periods in AT, and horizontal wind disturbances with a vertical wavelength of about 3 km in AT. Before examining these disturbances further, information provided by vertical momentum flux, which is a key for the following analyses, is reviewed.

5. Vertical momentum flux

Gravity waves have been considered to be important for the wind system in the height region around the mesopause (Lindzen 1981; Matsuno 1982) and lower stratosphere (Tanaka and Yamanaka 1985; Palmer et al. 1986) due to deposit of the momentum into the background wind system through the wave breaking. Similarly, it is possible that generation and breaking of the gravity waves affect the typhoon structure. Vertical momentum flux associated with small-scale wind disturbances like gravity waves is directly estimated by the VHF radar observations. The most accurate estimate is obtained with the method introduced by Vincent and Reid (1983) using line-of-sight wind velocities that are measured by two beams tilted symmetrically around the zenith (Reid 1987).

The vertical momentum flux is represented using horizontal ($\mathbf{v}'_h$) and vertical (w') components of wind fluctuations as $\rho_0\overline{\mathbf{v}'_h w'}$, where ρ_0 is the basic atmospheric density. Note that the vertical momentum flux is a vector. Contribution of the forcing to the background flow induced by the small-scale disturbances $d\mathbf{U}/dt$ is given as

$$\frac{d\mathbf{U}}{dt} \equiv -\frac{1}{\rho_0}\frac{\partial \rho_0 \overline{\mathbf{v}'_h w'}}{\partial z}. \tag{1}$$

Assuming an internal gravity wave in a form of $\mathbf{v}'_h$, $w' \propto \exp i(\mathbf{k}\cdot\mathbf{x} + mz - \omega_{\text{obs}}t)$, the continuity equation under the Boussinesq approximation becomes

$$\mathbf{k}\cdot\mathbf{v}'_h + mw' = 0, \tag{2}$$

where $\mathbf{k}$, m, and ω_{obs} are the horizontal wavenumber vector, vertical wavenumber, and observed frequency, respectively. Using (2) the vertical momentum flux is expressed as

$$\rho_0\overline{\mathbf{v}'_h w'} = -\rho_0 \frac{\mathbf{k}}{m}\overline{|\mathbf{v}'_{hp}|^2}, \tag{3}$$

where the overbars denote the spatial and temporal mean and $\mathbf{v}'_{hp}$ is a fluctuating horizontal wind component parallel to the horizontal wavenumber vector. When the intrinsic frequency $\hat{\omega}$ is restricted to the positive without losing any generality, a gravity wave propagating upward (downward) has negative (positive) m (e.g., Hirota and Niki 1985). Thus, the gravity wave propagating energy upward (downward) has a horizontal wavenumber vector in the same (opposite) direction of the vertical momentum flux vector.

In the case of a stationary mountain wave, the intrinsic phase speed $\hat{\mathbf{c}} = \hat{\omega}\mathbf{k}/|k|^2$ is related to the background wind component perpendicular to the ridges $\mathbf{U}$ as

$$\hat{\mathbf{c}} = -\mathbf{U} \tag{4}$$

(e.g., Holton 1979). Since actual topography is usually composed of a lot of ridges in almost all directions, it

can be expected that dominant waves have the intrinsic phase speeds parallel to the background wind. Equations (3) and (4) suggest that the vertical momentum flux associated with mountain waves points in the direction opposite to the background wind.

6. Vertical wind disturbances with short periods in BT

As shown by the statistical analysis in section 4, there are strong vertical wind disturbances with short periods less than several tens of minutes in BT whose spectral structure has never been reported by previous studies. The disturbances appeared for about half a day in the whole observed height range expanding from the troposphere to the lower stratosphere, as found from Fig. 7. The vertical wind fluctuations are probably due to deep convection, whose presence in BT was shown in section 3. Some of the disturbances, however, must be due to gravity waves because they are seen also in the lower stratosphere. The energy source of the gravity waves in the lower stratosphere is likely to be deep convection in the troposphere.

Another possible source is topography in strong surface wind associated with the typhoon. The possibility is not the case, however, as the following shows. If the disturbances are due to topographically forced waves, they must not extend to the height region above a critical level having a horizontal wind velocity of nearly zero (in the present case, corresponding to a height of 20 km; see Fig. 3), which is contrary to the observation. Moreover, as noted in section 4, the present gravity waves do not have such spectral characteristics of topographically forced waves.

In order to see the effects of the gravity waves in the stratosphere on the typhoon, the vertical momentum flux is examined. Since the estimation error is determined by that of radial wind velocity, the vertical momentum flux is shown in Fig. 10 without a factor of ρ_0. Averaging for $\mathbf{v}'_h w'$ is substituted for by smoothing using low-pass filters with cutoff lengths of 6 km in height and 10 h in time so as to see the vertical and temporal variation as a whole. It should be noted that $\mathbf{v}'_h w'$ in the lower stratosphere points to the west-northwest uniformly, while the direction in the troposphere is almost random. The absolute value of $\mathbf{v}'_h w'$ in the lower stratosphere amounts to about 0.1–0.4 $m^2 s^{-2}$, which is as large as observed for the topographically forced waves (Sato 1990).

The increase of vertical momentum flux in Fig. 10 with height in the lower stratosphere can be explained by decrease of air density. For example, density-weighted vertical momentum fluxes at heights of 15, 17.5, and 20 km are 0.027, 0.032, and 0.028 kg $m^{-1} s^{-2}$, respectively, which are almost constant in height. Thus, (1) indicates that the gravity waves interact little with the background wind in the lower stratosphere. Rather important is the drag to the background wind due to the "generation" of gravity waves having such large vertical momentum flux that probably occurred in the troposphere. Cyclonic wind of the typhoon blew northwestward in BT at the MU radar site. The direction is the same as that of the vertical momentum flux associated with the gravity waves. This shows that the generation of the gravity waves works to make the cyclonic wind rotation of the typhoon weaker.

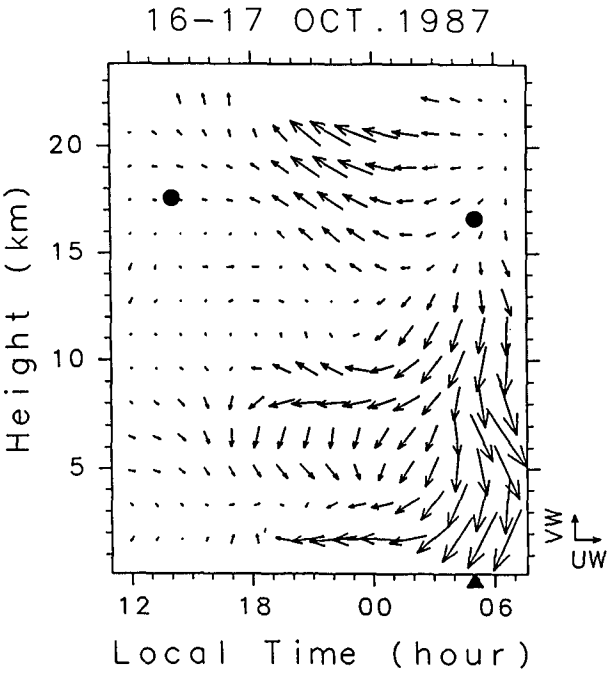

FIG. 10. A time–height section of vertical momentum flux vectors associated with fluctuations having periods less than 1 h in BT. Rightward and upward unit vectors show eastward and northward vertical momentum fluxes of 0.2 $m^2 s^{-2}$, respectively. A thick arrow on the horizontal axis indicates the time when the typhoon passed near the MU radar site. Circles denote the tropopause.

However the vertical momentum flux profile associated with the generation of gravity waves is masked by the random and large momentum flux due to deep convection in the troposphere, as found from Fig. 10. Thus, the drag is obtained using (1) by assuming the height region where the waves were excited. If the height region expands to 5 km around a height of 5 km, the drag amounts to about 0.7 m s^{-1} day^{-1} using the mean density-weighted vertical momentum flux of 0.03 kg $m^{-1} s^{-2}$ for the lower stratosphere. It should be noted that the order of estimation is unchanged by assumed depth of the height region because it affects only by the minus first power [see (1)].

Tropical cyclones can keep their structure owing to the production of kinetic energy by supply of sensible and latent heat to the center over the ocean, which compensates the energy dissipation by surface friction (e.g., Ooyama 1982). For a vortex with small scale

compared with the Rossby radius–like typhoons, the spindown time t_{spin} is expressed as

$$t_{spin} = H\sqrt{2/(f\nu)}, \quad (5)$$

where H is the depth of vortex, f is the inertial frequency, and ν is the kinematic viscosity (e.g., Holton 1979). Using typical values of 10 km for H, 10^2 m^2 s^{-1} for ν, and 10^{-4} for f, t_{spin} is estimated at about two days. This indicates that the drag by the surface friction is about 20–30 m s^{-1} day^{-1}.

The drag estimated for the observed gravity waves is several percent of the surface friction, and therefore, it is found that the generation of gravity waves is never a negligible mechanism to reduce the wind energy of the typhoon. Moreover, the gravity waves may play an important role in the middle and upper atmosphere, for example, in the generation of large-scale waves, through deposit of the momentum by dissipation. It was reported by Hung and Kuo (1978) that gravity waves with similar periods of a few minutes were observed in the ionosphere in association with a hurricane.

The ratio of vertical wind variance and vertical momentum flux corresponds to the aspect ratio α,

$$\alpha = k/m, \quad (6)$$

of the gravity waves, as found from (2). Since the vertical wind variance is about 0.15 m^2 s^{-2} independent of height (not shown here in detail) in the lower stratosphere, the aspect ratio is inferred to be about unity. This estimate is in accord with the fact that the dominant observed frequency is as high as Brunt–Väisälä frequency (1/5 min^{-1} for typical value in the stratosphere). Since the background wind in the lower stratosphere was weak (see Fig. 3), the observed frequency is almost equal to the intrinsic one. The dispersion relation for a gravity wave with intrinsic frequency of $\hat{\omega} \leqslant N$,

$$\hat{\omega}^2 = \frac{N^2k^2}{m^2 + k^2}, \quad (7)$$

indicates that almost unity aspect ratio means very high intrinsic (and observed in this case) frequency of $\hat{\omega} \approx \sqrt{2}N$. The gravity waves with such large aspect ratio are likely to have small horizontal wavelengths much less than hundreds of kilometers. According to an analysis by S91, however, the vertical wind fluctuations due to the gravity waves are almost in phase in vertical in the observed stratospheric region expanding several kilometers, so that the horizontal wavelength cannot be determined exactly.

7. Vertical wind disturbances with long periods in AT

In order to examine vertical wind disturbances with long periods more than several hours in AT, original vertical wind data are smoothed by a low-pass filter with a cutoff period of 5 h. The time–height section is shown as a contour map in Fig. 11. Large fluctuations are observed in the lower troposphere for about 40 h around the typhoon passage and in the upper troposphere after 0000 LST 17. In particular, strong upward motion more than 1 m s^{-1} lasting about 4 h is observed in the middle troposphere at the typhoon passage. As mentioned in section 4, vertical winds estimated in BT below a height of 5 km may be biased toward minus due to contamination of echo from rain drops. However the existence of disturbance in BT is confirmed by the appearance of large "positive" vertical wind components.

There are no tall convective clouds after 0400 LST 17 as found from the echo power profile (Fig. 4), although the rainfall rate seen in Fig. 5 is high until early AT. Thus, the disturbance reaching the tropopause in AT, including the strong upward motion at the typhoon passage (0500 LST 17), must not be due to convection, while the disturbance in BT may be due to convection having vertical motions fluctuating in a wide range of frequencies. Although there might be other possibilities, such as some kinds of instabilities associated with a drastic change in atmospheric stability at the typhoon passage, the most likely interpretation proposed here is that the disturbances in AT are due to mountain waves that ought to have been generated in strong surface wind associated with the typhoon over topography. It is shown in what follows that the interpretation does not contradict any observed features.

Characteristics of the disturbance agree well with mountain waves: the power of the disturbance is distributed largely near the surface. The power spectra are similar in shape and magnitude to those for mountain waves observed by the VHF radars (Ecklund et al. 1985; Sato 1990) as shown in section 4. Little disturbance appear above a critical level of about 20 km for stationary mountain waves. Since the vertical scale of the disturbance is large, Eq. (7) indicates their high intrinsic frequencies if the disturbance is due to gravity waves. This fact and very low observed frequencies of the disturbances indicate that the disturbance must be Doppler shifted largely by the background, which is also consistent with mountain waves.

Moreover, it is important that the disturbance ceased once around 1000 LST 17 and subsequently strengthened again. At the pause of the disturbance, the surface wind weakened (Fig. 3) and blew from the west of the radar site where there are no high mountains, as is found from a map of topography (Fig. 12). This feature further supports the view of mountain waves. It should be noted that the mountains over which this disturbance is excited are different from those examined by Sato (1990). The vertical wind disturbance analyzed by Sato was due to the gravity waves generated by a monsoon burst from the Siberian high in winter over mountains 100–200 km west-northwest of the MU radar site.

FIG. 11. Vertical wind components with periods longer than 5 h. Solid and dashed lines show positive and negative velocities, respectively. Contour interval is 0.25 m s^{-1}. A thick arrow on the horizontal axis indicates the time when the typhoon passed near the MU radar site. Circles and triangles denote the tropopause and inversion layer, respectively.

It is important that there is no large disturbance in BT in the upper troposphere in spite of strong wind near the surface observed in BT as well as in AT. The difference in vertical distribution of the disturbances between BT and AT may be attributable to the difference in atmospheric stability. Large energy dissipation process is expected in BT when convective activity is large.

Figure 13 presents vertical profiles of the turbulent energy dissipation rate (ϵ) estimated using spectral width of the atmospheric echo observed by the MU radar. Solid and dashed lines show ϵ for BT and AT, respectively. The spectral width of atmospheric echo can be broadened by other effects than atmospheric turbulence, that is, finite beamwidth of the radar, vertical shear of wind, and gravity waves with short periods comparable to the period for one wind measurement (about one minute in the present observation). The contamination to the spectral width is removed by the method introduced by Hocking (1983, 1988) to obtain accurate energy dissipation rate. For BT, only spectral width data obtained when upward motion was observed were used so as to avoid contamination due to echo by raindrops. A continuous profile around a freezing level of 5 km supports little effect of the contamination of rains and snows on the estimation.

The turbulent energy dissipation rate in the lower and middle troposphere in BT is about five times larger than in AT. Thus, it is likely that the gravity waves excited by topographic effects in BT lost their energy by large dissipation during their propagation before reaching the upper troposphere.

As expected from some studies of mountain waves (e.g., Lilly and Kennedy 1973; Sato 1990), the present vertical wind disturbances may associate with large vertical momentum flux and have a large effect on the background wind through their dissipation. Unfortunately, however, meaningful results could not be obtained because it is difficult to distinguish the disturbance from the background, including typhoon structure with similar vertical and time scales.

8. Horizontal wind disturbances observed in AT

The horizontal wind disturbances with a vertical wavelength of 3 km in AT are apparently seen in the unfiltered time–height sections of zonal and meridional wind components (Fig. 14), where some of the phase lines are shown by solid and dashed lines. Since these wavelike disturbances have long periods more than 6 h, further examination in this section is made for wind components with vertical wavelengths of 1.5–4.5 km and periods longer than 4 h. Figures 15a and 15b present the zonal and meridional components, respectively. The vertical wind component is not shown because there is no corresponding wavelike structure.

FIG. 12. A map of topography around the MU radar site. Contour interval is 250 m.

Through a hodograph analysis in a framework of inertio–gravity waves, S91 showed that the waves propagate their energy upward and downward from an inversion layer in the middle troposphere denoted by triangles in Fig. 15. The region surrounded by thick lines is filled with gravity waves propagating downward. Although validity of the assumption of inertio–gravity waves has not been confirmed, it is interesting to investigate them further. As mentioned in section 5, vertical momentum flux provides us with useful information on the disturbances.

Figure 15c shows the profiles of vertical momentum flux associated with the horizontal wind disturbances. Judged from the direction and vertical distribution, the disturbances are divided into four groups in the time–height section. One interesting feature is that the vertical momentum flux points to opposite directions above and below the inversion layer, namely, southward in B and northward in C. If the disturbances are due to inertio–gravity waves propagating upward in B and downward in C as suggested by S91, Eq. (3) indicates that horizontal wavenumber vectors of the gravity waves observed both above and below the inversion layer point to the south, and hence the gravity waves propagate southward relative to the background wind (outward from the typhoon).

Convergence of the momentum flux around the inversion layer suggests the existence of forcing to the background wind there, which does not depend on whether the disturbances are due to gravity waves or not. The forcing is estimated to be 4.0 m s^{-1} day^{-1} from (1) using values at heights of 8 and 10 km. Since the direction is northward, the forcing acts to weaken the cyclonic winds of the typhoon, similar to the disturbances analyzed in section 6.

It was shown in section 3 that the inversion layer corresponds to an end of the extratropical tropopause. Similar wave generation around the tropopause was reported by Sato (1989) using wind data obtained by the MU radar when a synoptic-scale pressure trough passed. She suggested that the generation mechanism is likely to be shearing instability around the tropopause. In order to examine the stability around the inversion layer, vertical shear of the background horizontal wind

$$\frac{dV}{dz} = \left[\left(\frac{du}{dz}\right)^2 + \left(\frac{dv}{dz}\right)^2\right]^{1/2}, \tag{8}$$

square of the Brunt–Väisälä frequency N^2, and the Richardson number

$$\mathrm{Ri} = N^2 \Big/ \left(\frac{dV}{dz}\right)^2 \tag{9}$$

are calculated using winds measured by the MU radar and temperature by a radiosonde launched at the radar site at 1100 LST 17 when the wavelike disturbances are dominant. The results are plotted in Fig. 16 as a function of height. The Brunt–Väisälä frequency is low, around a height of 8.5 km, and the wind shear is large below the inversion layer (9.5 km), which makes a thin layer with small Richardson number near the inversion layer. Although the minimum value is not so small as 0.25, which is the threshold for shearing instability, the atmosphere may have been unstable locally near the inversion layer. The disturbances in B and C are likely generated around the inversion layer due to the shearing instability.

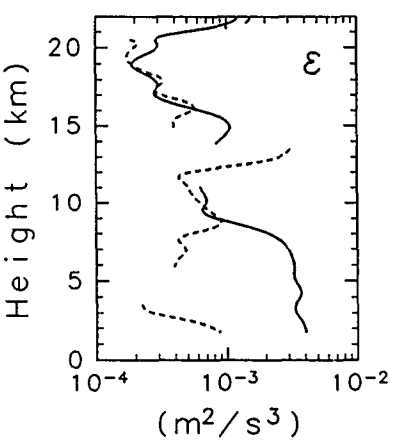

FIG. 13. Vertical profiles of the turbulent energy dissipation rate (ϵ). Solid and dashed lines show ϵ for BT and AT, respectively.

FIG. 14. Time–height sections of original (a) zonal and (b) meridional winds in AT.

FIG. 15. Time–height sections of (a) zonal and (b) meridional wind components of disturbances with a vertical wavelength of 3 km in AT. Contour interval is 2 m s^{-1}. Light and dark hatches show positive and negative wind velocities, respectively. Vertical momentum flux vectors associated with the disturbances are also presented (c), for which a smoothing was made by a low-pass filter with a cutoff length of 10 h instead of the average so as to see temporal and vertical variation of the vertical momentum flux. Rightward and upward unit vectors show eastward and northward vertical momentum fluxes of 0.1 m^2 s^{-2}, respectively. A thick arrow on the horizontal axis indicates the time when the typhoon passed near the MU radar site. Circles and triangles denote the tropopause and inversion layer, respectively.

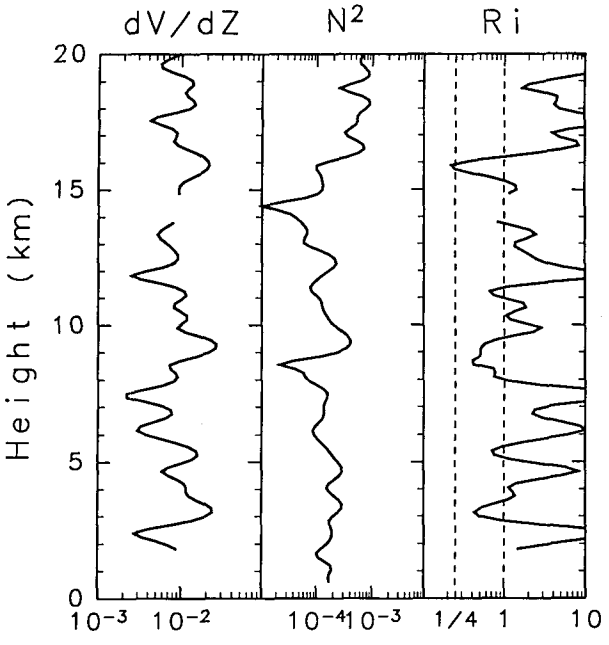

FIG. 16. Vertical profiles of vertical shear of horizontal wind (s^{-1}), square of the Brunt–Väisälä frequency (s^{-2}), and the Richardson number at 1100 LST 17.

On the other hand, vertical momentum flux vectors in D rotate clockwise in time. The direction is always opposite to the background wind (Fig. 3). This feature and (4) suggest that the disturbance in D is due to mountain waves with small vertical wavelengths. The vertical wavenumber m of a mountain wave in the background wind U is expressed under the hydrostatic approximation and ignoring vertical shear of the background wind as

$$m = \frac{N}{U} \tag{10}$$

(e.g., Gill 1982). Thus, vertical wavelengths of stationary gravity waves in weak wind near the surface can be as small as observed in Figs. 15a and 15b. The vertical momentum flux around 0000 LST 17 is small compared with the other periods. This is probably because the background wind is too large to make such mountain waves with short wavelengths as are extracted by a vertical filter used in this section.

Horizontal wind disturbances in A are distributed around and above the tropopause denoted by circles. Thus, the direct effect on the typhoon structure through the divergence of vertical momentum flux may be small. However, there is no doubt that generation of the gravity wave is closely related to the typhoon in a viewpoint of the timing of appearance. Although such monochromatic disturbances with a short vertical wavelength of 1–3 km have been frequently observed in the stratosphere, there are only a few case studies on the disturbances (Yamanaka et al. 1989; Ushimaru and Tanaka 1990), and the sources have been unknown. Thus, the disturbance in A is worth examining in relation to the typhoon.

Since this disturbance is highly monochromatic for about 15 h, we can estimate the wave parameters assuming that the disturbance is due to an inertio–gravity wave. The observed frequency ω_{obs} and vertical wavenumber m are directly estimated from Fig. 15a and 15b at about $2\pi/(20\text{ h})$ and $2\pi/(2.7\text{ km})$, respectively. The intrinsic frequency $\hat{\omega}$ is obtained through a hodograph analysis (Hirota and Niki 1985). Figure 17 gives an example for the inertio–gravity wave at 1400 LST 17. The ratio of long to short axes of the elliptic hodograph is equal to that of $\hat{\omega}$ to f. Thus, using the ratio observed in the hodograph (about 2.2) and f at the MU radar site [$2\pi/(21\text{ h})$], $\hat{\omega}$ is estimated to be about $2\pi/(9\text{ h})$. The hodograph provides the other information on the wave characteristics. Clockwise rotation with increasing height observed in the hodograph of Fig. 17 indicates that the wave propagates energy upward. The direction of the long axis of the ellipse gives direction of the horizontal wavenumber vector although an ambiguity remains for the sign. The vertical momentum flux associated with the inertio-gravity wave (Fig. 15c) shows that the horizontal wavenumber vector points to the southwestward, which is well in accord with the estimation by the hodograph.

In the following analysis, the direction of the horizontal wavenumber vector is fixed to be positive. The horizontal wavelength ($2\pi/k$) is estimated at about 300 km using the dispersion relation for an inertio-gravity wave:

$$\hat{\omega}^2 = f^2 + \frac{N^2k^2}{m^2}, \quad \hat{\omega} \geq f. \tag{11}$$

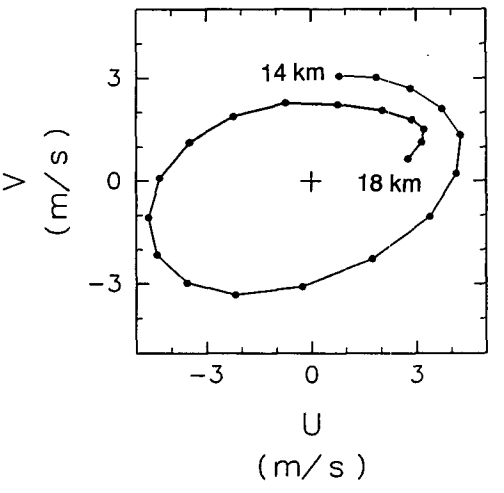

FIG. 17. A hodograph for an inertio–gravity wave observed in a height region of 14–18 km at 1400 LST 17. Dots denote data points at a height interval of 150 m. Numerals denote heights. Thicker lines show higher altitudes.

We used $2\pi/(5\text{ min})$ for N, which is a typical value in the stratosphere. The intrinsic frequency $\hat{\omega}$ is related to ω_{obs} by the background wind in the direction of the horizontal wavenumber vector U as

$$\hat{\omega} = \omega_{obs} - Uk, \tag{12}$$

where the Doppler shift by the vertical component of background wind is ignored. From this equation U is estimated at about -6 m s^{-1}, which is in good agreement with the observed background wind (~ -10 m s^{-1}) shown in Fig. 3. The amplitude of the horizontal wind component of the gravity wave in the direction of horizontal wavenumber vector is about 4.5 m s^{-1}. Thus, the vertical momentum flux is estimated using (3) at 0.08 m^2 s^{-2}. This corresponds well with the estimation by the Vincent and Reid's method (Fig. 15c).

In this way we could obtain the horizontal wavenumber of the gravity wave and its direction without any inconsistency with the observed physical quantities. Therefore, it is likely that the disturbance in region A is due to an inertio–gravity wave. Using this information, the horizontal phase velocity

$$c \equiv \frac{\omega_{obs}}{k} \tag{13}$$

and the horizontal group velocity

$$c_g \equiv \frac{\partial \omega_{obs}}{\partial k} = \frac{N^2 k}{\hat{\omega} m^2} + U \tag{14}$$

are estimated to be about 5 and 3 m s^{-1}, respectively. These obtained parameters are summarized in Table 1 as event 8-A.

The gravity wave appeared at 0600 LST 17 just after the typhoon passed near the radar site. The obtained horizontal group velocity indicates that the inertio–gravity wave propagated southwestward, that is, away from the typhoon moving northeastward at a speed of 15 m s^{-1}. From the horizontal group velocity and duration of the gravity wave, the horizontal expanse of the wave packet that passed over the radar site is estimated at least 150 km.

9. An inertio–gravity wave in BT

A similar analysis assuming an inertio–gravity wave is made for another monochromatic disturbance observed in the lower stratosphere about one day before the typhoon passage, which can be clearly seen in horizontal wind vectors of Fig. 3 during a period from 0000 to 1400 LST 16 in a height range from 16 to 21 km. The gravity wave has a long period of about 6 h and a long vertical wavelength of about 6 km. The parameters are very peculiar because the typical period and vertical wavelength of the gravity waves observed in the lower stratosphere in normal weather conditions are longer than 10 h and 1–3 km, respectively (see Hirota and Niki 1986; Yamanaka et al. 1989; Ushimaru and Tanaka 1990, for examples of the MU radar observations). Therefore, it is natural to consider that generation of the gravity wave is closely related to the typhoon.

Time–height sections of three wind components and vertical momentum flux for the gravity wave are shown in Fig. 18. The components of the gravity wave are extracted by a temporal bandpass filter with cutoff lengths of 4 and 10 h and a vertical low-pass filter with a cutoff length of 4 km. It is found that the disturbance is also highly monochromatic for over 10 hours. The disturbance is dominant especially in the meridional component, which is consistent with the fact that the vertical momentum flux points to the north. The wavelike structure is clearly found even in the weak vertical component (about 0.03 m s^{-1}). Figure 19 shows a hodograph at 0700 LST 16. The clockwise rotation with height suggests that the inertio–gravity wave propagated energy upward.

The wave parameters obtained through the same hodograph analysis and theoretical consideration as made in the previous section are summarized in Table 1 as event 9. The parameters were estimated again without any inconsistency with all information obtained by the observation, indicating that this disturbance is due to an inertio–gravity wave. It is noteworthy that the estimated vertical wind component of 0.04 m s^{-1} is also in accord with the observed vertical wind component.

Since the horizontal group velocity is about 20 m s^{-1} and the duration of the gravity wave is over 10 h, the horizontal (meridional) expanse of the wave is about 1000 km. The horizontal group velocity is very large compared with a traveling speed of the typhoon (about 8 m s^{-1} when the wave was observed). This suggests that the gravity wave was generated in the typhoon located to the south of the radar site, propagated northward fast, and reached the radar site earlier than the typhoon.

TABLE 1. Parameters of observed inertial gravity waves. U_{est} and U_{obs} are estimated and observed horizontal wind velocity in the direction of horizontal wavenumber vector, respectively.

Event	$2\pi/\omega_{obs}$ (h)	$2\pi/\hat{\omega}$ (h)	$2\pi/k$ (km)	$2\pi/m$ (km)	C (m s^{-1})	C_g (m s^{-1})	U_{est} (m s^{-1})	U_{obs} (m s^{-1})	Direction of k	$\overline{u'w'}$ (m^2 s^{-2})
8-A	20	9	300	2.7	5	3	−6	−10	southwestward	0.08
9	5.9	8	600	6.0	30	20	5	3	northward	0.04

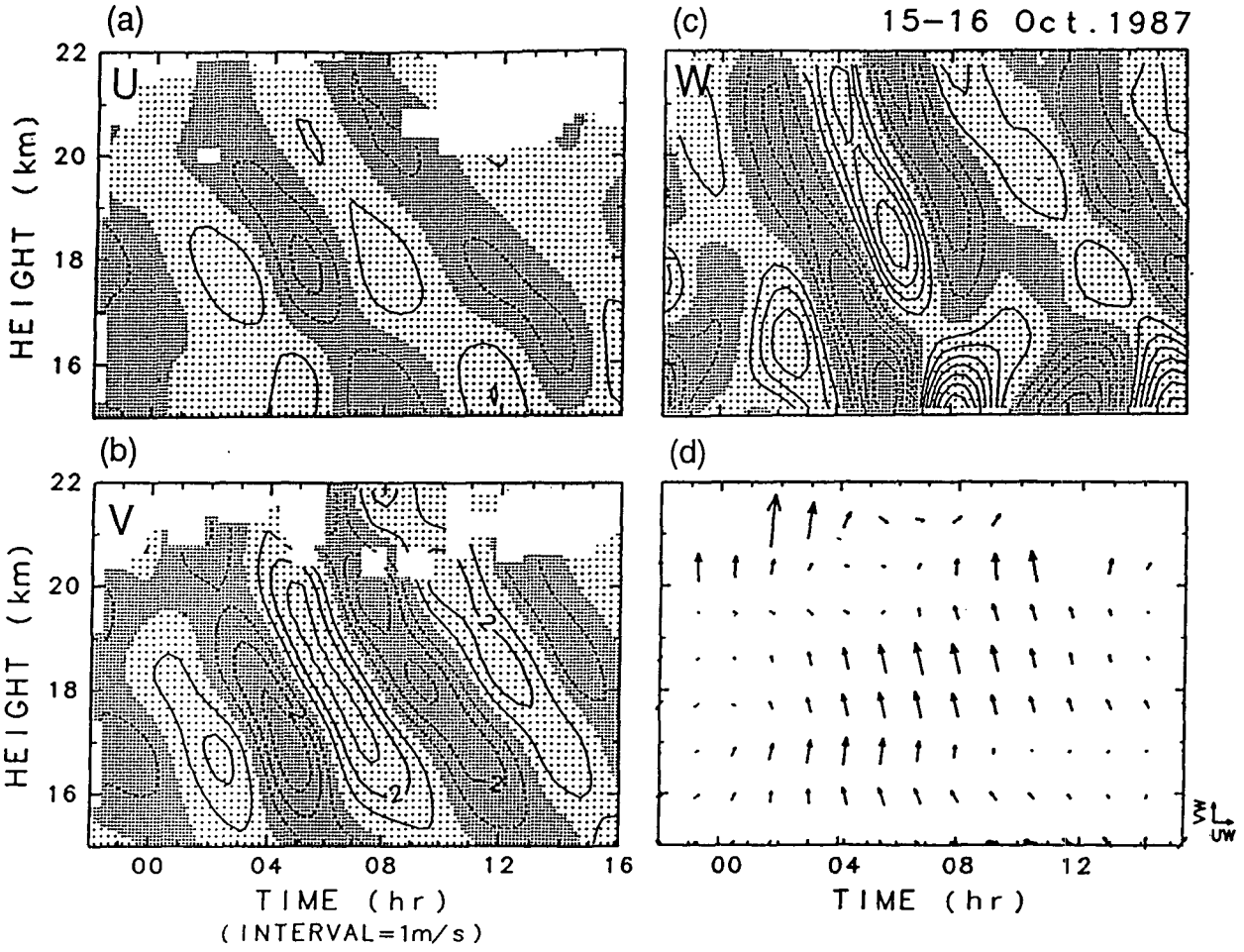

FIG. 18. A time–height section of (a) zonal, (b) meridional, and (c) vertical wind velocities and (d) vertical momentum flux vectors for an inertio–gravity wave observed about one day before the typhoon passage. Contour intervals are 1, 1, and 0.01 m s^{-1} for (a), (b), and (c), respectively. A smoothing was made for the vertical momentum flux by a low-pass filter with a cutoff length of 10 h. Rightward and upward unit vectors in (d) show eastward and northward vertical momentum fluxes of 0.05 m^2 s^{-2}.

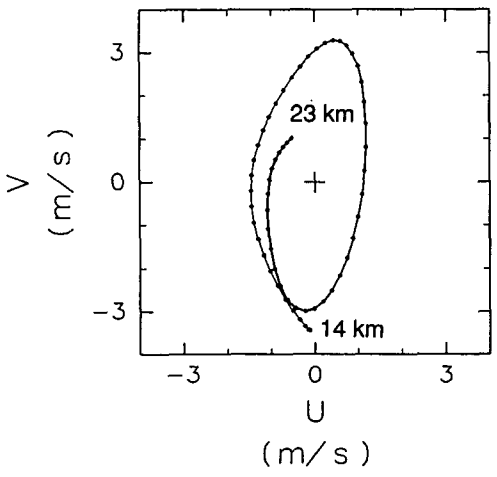

FIG. 19. As in Fig. 17 but for an inertio–gravity wave observed in a height region of 14–23 km at 0700 LST 16.

During the time when the inertio–gravity wave appeared, a rainband passed over the radar site that is shown as a stationary front in a weather chart at 0900 LST 16 in Fig. 2. The propagation speed of the rainband (10 m s^{-1}) is not in accord with either the horizontal group velocity or the horizontal phase velocity. Thus, it is not appropriate that the inertio–gravity wave is a part of the rainband structure. However, it is possible that the wave generation is related with the rainband.

10. Summary and concluding remarks

Through detailed analyses using observation data by the MU radar, several characteristics of small-scale wind disturbances associated with a typhoon have been revealed. The wind disturbances have been examined especially from the viewpoint of their relation with the

typhoon, considering generation, direction of propagation, and other effects on the typhoon.

First the atmospheric stability around the typhoon as the background of small-scale wind disturbances was examined. As a result it was found that convective activities in front of and behind the typhoon were very different and that the sharp boundary in convection was observed as a drastic change in the echo power profile of the MU radar when the center of the typhoon passed near the radar site.

Corresponding to the change in atmospheric stability, significant difference was found in statistical characteristics of the wind disturbances between periods before (BT) and after (AT) the typhoon passage. The difference was especially large for frequency power spectra of vertical wind fluctuations: dominant periods of the fluctuations were several tens of minutes in BT, while fluctuations in AT had long periods of several hours. The spectra obtained for BT were unique compared with other studies of vertical wind fluctuations observed by the VHF radars. Vertical wavenumber spectra indicated dominance of horizontal wind disturbances with a short vertical wavelength of about 3 km only in AT.

Further analysis was made of the several dominant small-scale wind disturbances in order to investigate their interaction with the typhoon and the possible sources. In particular, vertical momentum flux, which is directly calculated from the MU radar data, was used to examine horizontal direction of gravity wave propagation and exchange of momentum between the disturbances and the typhoon.

Vertical wind disturbances having short periods of several tens of minutes in BT were distributed in the whole observed height region. The gravity waves in the lower stratosphere had large vertical momentum flux comparable to that of topographically forced waves. The direction of vertical momentum flux showed that generation of the gravity waves has the effect of decelerating strong cyclonic wind on the typhoon in the troposphere. The gravity waves in the lower stratosphere are likely excited in association with deep convection in the troposphere.

Vertical wind disturbances with long periods of several hours in AT had characteristics of topographically forced gravity waves, that is, the time and vertical scales, spectral structure, vertical distribution of the power, and timing of the appearance. Absence of the disturbances in BT could be explained by a large dissipation process related to strong convection.

Horizontal wind disturbances having a vertical wavelength of about 3 km in AT were divided into several parts in the time–height section by their characteristics in vertical momentum flux. The disturbances around the inversion layer in the middle troposphere were associated with divergence of vertical momentum flux corresponding to a forcing to decelerate the cyclonic wind of the typhoon. The generation mechanism of the disturbances is likely to be sharing instability around the inversion layer. On the other hand, the direction of the vertical momentum flux in the lower troposphere changed clockwise. This indicates the possibility that the disturbances in the height region are due to gravity waves forced topographically in strong winds of the typhoon. The disturbance in the lower stratosphere was highly monochromatic for about 15 h. The timing of appearance suggests a close relation between the typhoon and the generation of the disturbances. The disturbance was considered to be an inertio–gravity wave, because the wave parameters were estimated without any inconsistency with all observed quantities. This inertio–gravity wave propagated energy upward and southwestward away from the typhoon.

Similar analysis was made for a highly monochromatic wavelike disturbance with a period of 6 h and vertical wavelength of 6 km lasting over 10 h in the lower stratosphere about one day before the typhoon passage. The characteristics were unique compared with those of gravity waves in the lower stratosphere reported in the previous studies using the MU radar data. Since the wave parameters were obtained without any inconsistency also in this case, the disturbance could be identified as an inertio–gravity wave. The estimated northward horizontal group velocity was larger than the traveling speed of the typhoon. This means that the gravity wave was generated in association with the typhoon when the typhoon was situated to the south of the islands of Japan, and reached the radar site earlier than the typhoon.

These disturbances are illustrated schematically in the time–height section of Fig. 20, which corresponds to the northeast–southwest section of the typhoon ignoring variation in time.

It should be noted that the short-period gravity waves in BT may be similar to those analyzed by Black (1977, 1983) using stereoscopic photographs of Hurricane Ellen in respect to their small horizontal wavelengths. Black (1977) showed that the wave energy flux was several percent of the total energy advection within 100 km of Hurricane Hilda estimated by Hawkins and Rubsam (1968), which is similar to the evaluation for drag due to gravity waves in BT made in section 6, while the compared physical value is not exactly the same. Black suggested a mechanism of the wave excitation whereby a deep penetration of convection acts like "a rock in a pond," radiating gravity waves outward. Such a distinctly large upward motion like a plume however, was not observed—at least over the MU radar site (see Fig. 7). Thus, the identification cannot be made.

As mentioned in section 1, Matsumoto and Okamura (1985) analyzed a pressure dip embedded in the northwestern quadrant of Typhoon Gay. The structure is consistent with the internal gravity wave in a two-dimensional two-layer model. An extremely sharp change was observed in time series of horizontal winds

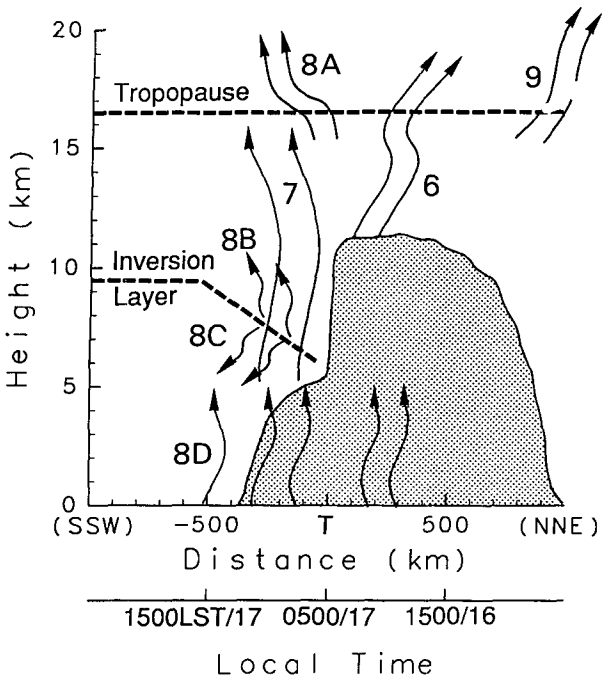

FIG. 20. A schematic picture of wind disturbances in association with Typhoon Kelly observed by the MU radar. Numerals in the figure show the section numbers where the disturbances were discussed. Shading shows a moist (nearly saturated) atmospheric region based on the radiosonde data.

as well as the surface pressure. The structure of the disturbance extended up to a height of about 5 km. These characteristics are not identical to any of the dominant wind disturbances examined in this study. The wind change associated with the pressure dip may have been dominated by convective motions or mountain waves with large amplitudes in the MU radar wind data if it existed. Studies using data of various quantities in various sections are important.

Throughout these case studies, it was found that the typhoon is significant as an energy source of gravity waves. One of the most interesting results in this study is that some of the gravity waves were generated so as to decelerate strong cyclonic wind of the typhoon although the estimated drag was only several percent of the surface friction. Topographically forced gravity waves, which could not be quantitatively examined in terms of interaction with the typhoon in this study, may also bring drag to the typhoon through the wave breaking in the upper troposphere. It is necessary to investigate the role of gravity waves on the decay of typhoons and/or the transformation of the typhoon into the extratropical cyclone.

It should be noted further that some of the gravity waves associated with the typhoon examined in this study (sections 6 and 9) appeared up to the top of observed height region, and hence, they may reach the upper-atmospheric region. Gravity waves in the upper mesosphere, which is another observable region by the MST radars, usually have longer vertical wavelengths than those in the lower stratosphere. For example, vertical wavelengths of inertio-gravity waves detected by Yamamoto et al. (1987) and Muraoka et al. (1988) are about 6 km, which is very similar to that of the inertio-gravity waves examined in section 9. This suggests the possibility that a typhoon is one of the important sources of gravity waves observed in the middle atmosphere.

Acknowledgments. This paper is a part of K. Sato's doctoral dissertation. She gratefully acknowledges the support and guidance of her advisor, Professor Isamu Hirota. Special thanks are due to Drs. Masanori Yamasaki, Manabu D. Yamanaka, and Toshitaka Tsuda for their fruitful discussion and comments. Thanks are extended to Dr. Toru Sato for his providing the valuable MU radar data, useful discussion on the data accuracy, and encouragement to perform this study. The author appreciates two reviewers for their several appropriate comments. The Radar-AMeDAS Composite Charts were graciously supplied by Dr. Yukio Misumi at the Japan Meteorological Agency. The MU radar belongs to and is operated by the Radio Atmospheric Science Center of Kyoto University.

REFERENCES

Abdullah, A. J., 1966: The spiral bands of a hurricane: A possible dynamic explanation. *J. Atmos. Sci.*, **23**, 367–375.

Battan, L. J., 1973: *Radar Observation of the Atmosphere.* The University of Chicago Press, 324 pp.

Black, P. G., 1977: Some aspects of tropical storm structure revealed by hand-held camera photographs from space. *Skylab Explores the Earth,* National Aeronautics and Space Administration, SP-380, 417–461.

——, 1983: Tropical storm structure revealed by stereoscopic photographs from Skylab. *Adv. Space Res.*, **2**, 115–224.

Brown, P. R. A., 1983: Aircraft measurements of mountain waves and their associated flux over the British Isles. *Quart. J. Roy. Meteor. Soc.*, **109**, 849–866.

Dewan, E. M., and R. E. Good, 1986: Saturation and the "universal" spectrum for vertical profiles of horizontal scalar winds in the atmosphere. *J. Geophys. Res.*, **6**, 976–981.

Ecklund, W. L., K. S. Gage, and A. C. Riddle, 1981: Gravity wave activity in vertical winds observed by the Poker Flat MST radar. *Geophys. Res. Lett.*, **8**, 285–288.

——, K. S. Gage, B. B. Balsley, R. G. Strauch, and J. L. Green, 1982: Vertical wind variability observed by VHF radar in the lee of the Colorado Rockies. *Mon. Wea. Rev.*, **110**, 1451–1457.

——, B. B. Balsley, D. A. Carter, A. C. Riddle, M. Crochet, and R. Garello, 1985: Observation of vertical motions in the troposphere and lower stratosphere using three closely spaces ST radars. *Radio Sci.*, **20**, 1196–1206.

——, K. S. Gage, G. D. Nastrom, and B. B. Balsley, 1986: A preliminary climatology of the spectrum of vertical velocity observed by clear-air Doppler radar. *J. Climate Appl. Meteor.*, **25**, 885–892.

Fukao, S., T. Sato, T. Tsuda, S. Kato, K. Wakasugi, and T. Makihira, 1985a: The MU radar with an active phased array system, 1. Antenna and power amplifiers. *Radio Sci.*, **20**, 1155–1168.

——, T. Tsuda, T. Sato, S. Kato, K. Wakasugi, and T. Makihira, 1985b: The MU radar with an active phased array system, 2. In-house equipment. *Radio Sci.*, **20**, 1169–1176.

——, K. Wakasugi, T. Sato, S. Morimoto, T. Tsuda, I. Hirota, I. Kimura, and S. Kato, 1985c: Direct measurement of air and

precipitation particle motion by very high frequency Doppler radar. *Nature,* **316,** 712–714.
——, M. D. Yamanaka, H. Matsumoto, T. Sato, T. Tsuda, and S. Kato, 1989: Wind fluctuations near a cold vortex–tropopause funnel system observed by the MU radar. *Pure Appl. Geophys.,* **130,** 463–479.
Gill, A. E., 1982: *Atmosphere–Ocean Dynamics.* Academic Press, 662 pp.
Hawkins, H. F., and D. T. Rubsam, 1968: Hurricane Hilda, 1964: II. Structure and budgets of the hurricane on October 1, 1964. *Mon. Wea. Rev.,* **96,** 617–636.
Hines, C. O., 1991: The saturation of gravity waves in the middle atmosphere. Part I: Critique of linear-instability theory. *J. Atmos. Sci.,* **48,** 1348–1359.
Hirota, I., and T. Niki, 1985: A statistical study of inertia-gravity waves in the middle atmosphere. *J. Meteor. Soc., Japan,* **63,** 1055–1066.
——, and ——, 1986: Inertia-gravity waves in the troposphere and stratosphere observed by the MU radar. *J. Meteor. Soc., Japan,* **64,** 995–999.
Hocking, W. K., 1983: On the extraction of atmospheric turbulence parameters from radar backscatter Doppler spectra—I. Theory. *J. Atmos. Terr. Phys.,* **45,** 89–102.
Hocking, W. K., 1985: Measurement of turbulent energy dissipation rates in the middle atmosphere by radar techniques: a review. *Radio Sci.,* **20,** 1403–1422.
——, 1988: Two years of continuous measurements of turbulence parameters in the upper mesosphere and lower thermosphere made with a 2-MHz radar. *J. Geophys. Res.,* **93,** 2475–2491.
Hoinka. K. P., 1984: Observation of a mountain wave event over the Pyrenees. *Tellus,* **36A,** 369–383.
——, 1985: Observation of the airflow over the Alps during a foehn event. *Quart. J. Roy. Meteor. Soc.,* **111,** 199–224.
Holton, J. R., 1979: *An Introduction to Dynamic Meteorology.* Academic Press, 391 pp.
Hung, R. J., and J. P. Kuo, 1978: Ionospheric observation of gravity-waves associated with Hurricane Eloise. *J. Geophys.,* **45,** 67–80.
——, Y. D. Tsao, D. L. Johnson, S. J. Chen, C. H. Lin, J. M. Cheng, and C. M. You, 1988: VHF radar remote sensing of atmospheric parameters over Taiwan during the time period of typhoon Wayne. *Int. J. Remote Sensing,* **9,** 477–493.
Kurihara, Y., 1976: On the development of spiral bands in a tropical cyclone. *J. Atmos. Sci.,* **33,** 940–958.
Lilly, D. K., and P. J. Kennedy, 1973: Observations of a stationary mountain wave and its associated momentum flux and energy dissipation. *J. Atmos. Sci.,* **30,** 1135–1152.
——, J. M. Nicholls, R. M. Chervin, P. J. Kennedy, and J. B. Klemp, 1982: Aircraft measurements of wave momentum flux over the Colorado Rocky mountains. *Quart. J. Roy. Meteor. Soc.,* **108,** 625–642.
Lindzen, R. S., 1981: Turbulence and stress due to gravity wave and tidal breakdown. *J. Geophys. Res.,* **86,** 9707–9714.
Matsumoto, S., and H. Okamura, 1985: The internal gravity wave observed in the Typhoon T8124 (Gay). *J. Meteor. Soc. Japan,* **63,** 37–51.
Matsuno, T., 1982: A quasi one-dimensional model of the middle atmosphere circulation interacting with internal gravity waves. *J. Meteor. Soc. Japan,* **60,** 215–226.
Muraoka, Y., T. Sugiyama, K. Kawahira, T. Sato, T. Tsuda, S. Fukao, and S. Kato, 1988: Formation of mesospheric VHF echoing layers due to a gravity wave motion. *J. Atmos. Terr. Phys.,* **50,** 819–829.
Ooyama, K. V., 1982: Conceptual evolution of the theory and modeling of the tropical cyclone. *J. Meteor. Soc. Japan,* **60,** 369–380.
Palmer, T. N., G. J. Shutts, and R. Swinbank, 1986: Alleviation of a systematic westerly bias in general circulation and numerical weather prediction models through an gravity wave drag parameterization. *Quart. J. Roy. Meteor. Soc.,* **112,** 1001–1039.
Reid, I. M., 1987: Some aspects of Doppler radar measurements of the mean and fluctuating components of the wind field in the upper middle atmosphere. *J. Atmos. Terr. Phys.,* **49,** 467–484.
Sato, K., 1989: An internal gravity wave associated with a synoptic-scale pressure trough observed by the MU radar. *J. Meteor. Soc. Japan,* **67,** 325–334.
——, 1990: Vertical wind disturbances in the troposphere and lower stratosphere observed by the MU radar. *J. Atmos. Sci.,* **47,** 2803–2817.
Sato, T., N. Ao, M. Yamamoto, S. Fukao, T. Tsuda, and S. Kato, 1991: A typhoon observed with the MU radar. *Mon. Wea. Rev.,* **119,** 755–768.
Smith, S. A., D. C. Fritts, and T. E. VanZandt, 1987: Evidence of a saturation spectrum of atmospheric gravity waves. *J. Atmos. Sci.,* **44,** 1404–1410.
Tanaka, H., and M. D. Yamanaka, 1985: Atmospheric circulation in the lower stratosphere induced by the mesoscale mountain wave breakdown. *J. Meteor. Soc. Japan,* **63,** 1047–1054.
suda, T., T. Inoue, D. C. Fritts, T. E. VanZandt, S. Kato, T. Sato, and S. Fukao, 1989: MST radar observations of a saturated gravity wave spectrum. *J. Atmos. Sci.,* **46,** 2440–2447.
Uccellini, L. W., and S. E. Koch, 1987: The synoptic setting and possible energy sources for mesoscale wave disturbances. *Mon. Wea. Rev.,* **115,** 721–729.
Ushimaru, S., and H. Tanaka, 1990: Characteristics of internal inertial gravity waves and inertial waves in the lower stratosphere observed by the MU radar. *J. Meteor. Soc. Japan,* **68,** 1–18.
Vincent, R. A., and I. M. Reid, 1983: HF Doppler measurements of mesospheric gravity wave momentum fluxes. *J. Atmos. Sci.,* **40,** 1321–1333.
Wakasugi, K., A. Mizutani, M. Matsuo, S. Fukao, and S. Kato, 1986: A direct method for deriving drop-size distribution and vertical air velocities from VHF Doppler radar spectra. *J. Atmos. Oceanic Technol.,* **3,** 623–629.
Wakasugi, K., A. Mizutani, M. Matsuo, S. Fukao, and S. Kato, 1987: Further discussion on deriving drop-size distribution and vertical air velocities directly from VHF Doppler radar spectra. *J. Atmos. Oceanic Technol.,* **4,** 170–179.
Willoughby, H. E., F. D. Marks, and R. J. Feinberg, 1984: Stationary and moving convective bands in hurricanes. *J. Atmos. Sci.,* **41,** 3189–3211.
Xu, W., 1983: Unstable spiral inertial gravity waves in typhoons. *Sci. Sinica.,* **26,** 70–80.
Yamamoto, M., T. Tsuda, S. Kato, T. Sato, and S. Fukao, 1987: A saturated inertia gravity wave in the mesosphere observed by the middle and upper atmosphere radar. *J. Geophys. Res.,* **92,** 11 993–11 999.
Yamamoto, R., 1963: A dynamical theory of spiral rain band in tropical cyclones. *Tellus,* **15,** 153–161.
Yamanaka, M. D., S. Fukao, H. Matsumoto, T. Sato, T. Tsuda, and S. Kato, 1989: Internal gravity wave selection in the upper troposphere and lower stratosphere observed by the MU radar: Preliminary results. *Pure Appl. Geophys.,* **130,** 481–495.
Yamasaki, M., 1986: A three-dimensional tropical cyclone model with parameterized cumulus convection. *Papers in Meteor. Geophys.,* **37,** 205–234.